

# Nanoscale

Accepted Manuscript



This is an *Accepted Manuscript*, which has been through the Royal Society of Chemistry peer review process and has been accepted for publication.

*Accepted Manuscripts* are published online shortly after acceptance, before technical editing, formatting and proof reading. Using this free service, authors can make their results available to the community, in citable form, before we publish the edited article. We will replace this *Accepted Manuscript* with the edited and formatted *Advance Article* as soon as it is available.

You can find more information about *Accepted Manuscripts* in the [Information for Authors](#).

Please note that technical editing may introduce minor changes to the text and/or graphics, which may alter content. The journal's standard [Terms & Conditions](#) and the [Ethical guidelines](#) still apply. In no event shall the Royal Society of Chemistry be held responsible for any errors or omissions in this *Accepted Manuscript* or any consequences arising from the use of any information it contains.

NaYF<sub>4</sub>: Yb,Tm Nanocrystals and TiO<sub>2</sub> Inverse Opal Composite Films: A  
Novel Device for Upconversion Enhancement and Solid-based Sensing of  
Avidin

Sai Xu<sup>†</sup>, Wen Xu<sup>†</sup>, Yunfeng Wang<sup>†</sup>, Shuang Zhang<sup>†</sup>, Yongsheng Zhu<sup>†</sup>, Li Tao<sup>†</sup>, Lei  
Xia<sup>†</sup>, Pingwei Zhou<sup>†</sup>, Hongwei Song<sup>\*†‡</sup>

<sup>†</sup>State Key Laboratory on Integrated Optoelectronics, College of Electronic Science  
and Engineering, Jilin University, 2699 Qianjin Street, Changchun, 130012,  
People's Republic of China.

<sup>‡</sup>The State Key Laboratory of Bioelectronics, Southeast University, 210096 P. R.  
China

Corresponding to: Prof. Hongwei Song

*State Key Laboratory on Integrated Optoelectronics,*

*College of Electronic Science and Engineering, Jilin University*

Email: songhw@jlu.edu.cn

*Phone and Fax: 86-431-85155129*

## Abstract

Upconversion luminescence (UCL) detection based on rare-earth doped upconversion nanocrystals (UCNCs) as probes has been proved to exhibit a large anti-Stokes shift, no autofluorescence from biological samples, and no photobleaching. However, it is still a challenge to achieve stable, reproducible of solid-based UCL bio-sensor because of ineffective UCL of the UCNCs. In this work, we fabricated TiO<sub>2</sub> inverse opal photonic crystals (IOPCs) /NaYF<sub>4</sub>:Yb<sup>3+</sup>, Tm<sup>3+</sup> (Er<sup>3+</sup>) UCNCs composite films, which can tremendously improve the overall UCL of Tm<sup>3+</sup> as high as 43-fold. Based on the fluorescence resonance energy transfer (FRET) and the specific interaction between biotin and avidin, a novel solid-based UC biosensor was presented for sensing avidin. This solid-based detection system is convenient for detection, and also can offer two parameters for detecting trace amount of avidin, namely, the emission intensity and the fluorescent decay time. The sensor is with high sensitivity of 34pmol<sup>-1</sup>, good linear relationship of 0.996 and low detection limit of 48 pmol. It also exhibits excellent long-time photostability, and absence of autofluorescence, and thus may have great potential for versatile applications in biodetection.

**Keywords:** Inverse opal composite films, Enhancement upconversion, Solid-based detection

## 1. Introduction

In recent years, nanocrystals (NCs) doped with trivalent lanthanide ions ( $\text{Ln}^{3+}$ ) have attracted extensive attention because of their outstanding properties such as large Stokes shift, sharp emissions, and long luminescent lifetimes.<sup>1,2</sup> Based on these outstanding properties,  $\text{Ln}^{3+}$  doped NCs play an important role in biomedical applications, display devices, optical communications, spectral conversion of solar cells and etc.<sup>3-6</sup> Among all the  $\text{Ln}^{3+}$  doped NCs, UCNCs, which can convert a low frequency excitation photon into a high frequency emission photon through two-photon or multi-photon processes have demonstrated various of front applications on biological and medical field.<sup>7</sup> Compared to the organic fluorophores and quantum dots (QDs) commonly used in the biological field, UCNCs possess various of advantages due to their unique anti-Stokes fluorescence properties, such as large penetration depth into tissues, low background noise as well as high chemical stability and low toxicity.<sup>8</sup> Until now, UCNCs have been extensive applied in vivo fluorescence labeling, photodynamic therapy of cancer, drug delivery, optical sensors for biodetecting temperature, pH value, and various biological matters.<sup>9-11</sup>

FRET is a nonradiative process characterized by ET between an excited donor and an acceptor through long-range dipole–dipole interaction. It is widely used as a spectroscopic ruler in biological detection.<sup>12,13</sup> The donor and acceptor fluorophores are linked in close proximity, typically less than a few nanometers, and the donor emission spectrum to overlap with the acceptor absorption. To achieve the detecting function, the UCNCs were commonly combined with other chromophores, such as

organic dyes, fluorescent proteins, and semiconductor.<sup>14,15</sup> Nowadays, several sensors based on FRET have been developed to detect DNA, metal ions, and small molecules, where the UCNCs (donor) transfer energy to other chromophores (acceptor) resulting in changes in UC emission intensity. Recently, Liu developed a combination of UCNCs and MnO<sub>2</sub> nanosheets for the selective detection of glutathione.<sup>16</sup> Similarly, Li. and his coworkers demonstrated a highly sensitive water-soluble nanosystem based on cyanine dye-assembled NaYF<sub>4</sub>:Yb<sup>3+</sup>, Er<sup>3+</sup>, Tm<sup>3+</sup> UCNCs for UCL sensing and bioimaging of methylmercury.<sup>17</sup> However, it should be highlighted that the above-mentioned UCNCs system sensors were all detected in the solution. The liquid-based sensors are usually unstable, irreproducible and with low UCL due to the interaction of UCNCs with solutions, which will affect the detection limit and sensitivity unavoidably. Therefore, it is significant to develop novel solid state UCL biosensors, which is permitted to work easily, stably and repeatedly.

The low UCL quantum yield is one of the bottleneck problems for the application of biosensors based on UCNCs. For instance, it was reported that the luminescent quantum yield of the most efficient  $\beta$ -phase NaYF<sub>4</sub>:Yb<sup>3+</sup>,Er<sup>3+</sup> microsized polycrystalline powders was only 3% under the excitation of 980 nm. And, the particles used for biodetection are usually with small size to ensure a large surface area to connect more biomolecules, but the UCL efficiency of NaLuF<sub>4</sub>: Tm<sup>3+</sup>, Yb<sup>3+</sup> UCNCs with sizes ranging of 10-20 nm is lower than 0.4%.<sup>18</sup> So it is important to enhance the emission intensity of the UCNCs for biological application. Up to now, numbers of methods have been developed to improve the efficiency of UCNCs, such

as the selection of suitable host and doping ions, surface modification, the device of core-shell structure, surface plasmon enhancement based on the interaction of UCNCs with noble metal NPs, such as gold, silver and etc.<sup>19-23</sup> Very recently, our group has explored novel strategies to improve the UCL of NaYF<sub>4</sub>:Yb, Er/Tm UCNCs, which is by the coupling of the UCNCs with PMMA photonic crystals (PCs) or hybrids of silver plasmon nanostructures and PMMA opal photonic crystals.<sup>24,25</sup> By these designs, a maximum enhancement of ~32 fold or ~60-fold was obtained, respectively. It is expected that the modulation of PCs on UCL of NaYF<sub>4</sub>:Yb, Er/Tm UCNCs could be easily applied on the device of biosensing.

In this work, we developed a novel complex of NaYF<sub>4</sub>: Yb, Tm UCNCs and TiO<sub>2</sub> inverse opal photonic crystals (IOPCs) for responsive sensing of avidin. Note that TiO<sub>2</sub> nanocrystalline has superior biological compatibility to biomolecules, since it is widely used in producing toothpaste and cosmetics. Besides it is also with optical transparency, and is preference of selective interaction with some proteins.<sup>26</sup> The porous inverse opal structure of TiO<sub>2</sub> and its dispersion to NaYF<sub>4</sub>:Yb<sup>3+</sup>,Er<sup>3+</sup>/Tm<sup>3+</sup> UCNCs not only could enhance the UCL, but also could ensure the large surface area to improve the effective connection of the UCNCs with avidin. An optimum UC enhancement factor (EF) of 43-fold was obtained for the overall UCL intensity of Tm<sup>3+</sup> with this unique strategy. And more, this complex was used as a sensitive solid-based UC sensor for the detection of avidin, which demonstrated more stable, convenient and applicable permanence than the liquid-based UC biosensor.

## 2. Experimental Section

### 2.1 Synthesis of NaYF<sub>4</sub>:Yb, Tm/Er.

OA-coated NaYF<sub>4</sub>:Yb,Tm/Er NCs were synthesized according to the typical solvothermal method.<sup>27</sup> The reaction temperature was controlled in the range of 285-330 °C to obtain different sizes of NaYF<sub>4</sub> NCs. The as-prepared products were collected and washed with absolute ethanol/cyclohexane (1:1 v/v) three times, and the final products were dissolved in the cyclohexane solution for following experiments.

### 2.2 Synthesis of water-soluble PEI-NaYF<sub>4</sub>:Yb, Tm NCs

PEI-modified water-soluble NaYF<sub>4</sub>:Yb,Tm NCs were synthesized via a solvothermal method following a procedure reported previously.<sup>28</sup> NaCl (2.5 mmol), PEI (0.4 g), Y(NO<sub>3</sub>)<sub>3</sub> (0.798 mmol), Yb(NO<sub>3</sub>)<sub>3</sub> (0.20 mmol), and Tm(NO<sub>3</sub>)<sub>3</sub> (0.002 mmol) was dissolved in EG (15 mL) under vigorous stirring. When the solution became transparent, NH<sub>4</sub>F (4 mmol) in EG (10 mL) was added to the solution. After stirred for another 10 min, the whole mixture was transferred into a 25 mL Teflon-lined stainless steel. The autoclave was sealed and heated under 200 °C for 2h hydrothermal treatment. After the autoclave cooled down to room temperature naturally, NaYF<sub>4</sub>: Yb, Tm NCs were harvested by centrifugation and washed with deionized water three times, and then redispersed in phosphate buffered saline (PBS). The NaYF<sub>4</sub>: Ce,Tb NCs (PEI-NaYF<sub>4</sub>: 5% Ce, 5% Tb) were synthesized by the same method.

### 2.3 Preparation of biotin-conjugated NaYF<sub>4</sub>

50 mg of PEI-NCs was diluted in 5 mL of PBS buffer solution (pH 7.4, 10 mM),

then added 5 mg of activated biotin to the mixture under gentle shaking for 4h of reaction at room temperature. Biotin was covalently conjugated with UCNCs by amido bond. Then the mixture was harvested with centrifugation and washed three times with PBS buffer solution to remove excess biotin. The bio-UCNCs was diluted in 5 mL of PBS and stored at 4 °C for further use.

#### **2.4 Synthesis of FITC-labeled avidin**

Prior to the detection, avidin was labeled with FITC following the well-established protocol. 10 mg avidin was dissolved in 5 mL of 0.1 M sodium carbonate buffer (pH 9.5). Meanwhile, 1.0 mg FITC was dissolved in 0.5 mL DMSO. Thereafter, the two solutions were mixed gently and the reaction was allowed to proceed overnight at 4 °C in the dark. The excess FITC was removed via dialysis for 48 h using a membrane of molecular weight cutoff of 14000 Da.

To investigate the fluorescence quenching degree, the as-prepared composite films were placed in the 24-well plates, subsequently, different amount of avidin-FITC solutions were dropwise added on the films. The films were incubated in the dark for 30 min, and then were subject to fluorescence measurement.

#### **2.5 Preparation of TiO<sub>2</sub> IOPCs**

The TiO<sub>2</sub> IOPCs were prepared by the solgel method with a PMMA latex sphere template technique. First, monodispersed PMMA latex spheres with controllable sizes were synthesized. Then, a thin-film template was self-assembled through the vertical deposition process. The colloid suspension (5% solid content) of PMMA microspheres was dropped onto a glass substrate and placed in a 32 °C oven for 24 h.

The PMMA colloidal spheres slowly self-organized into highly ordered colloidal arrays on the glass substrate, driven by surface tension of the liquid in the evaporating process. Following deposition, the opals were sintered for 40 min at 120 °C to enhance their physical strength. In the preparation of TiO<sub>2</sub> precursor sol, 10ml butyltitanate, 10ml ethanol, 1ml nitric acid were mixed and stirred for 1h to form a transparent solution. The prepared precursor solutions were used to infiltrate into the voids of the opal template through capillary force. After filtration, the resulting products were dried in air at room temperature. Annealing was carried out with slowly elevated temperature (1 °C /min) up to 500 °C for 3 h. By controlling the diameters of PMMA latex spheres during polymerization in the previous step, the photonic stop band (PSB) of IOPCs was finely tuned. Moreover, the TiO<sub>2</sub> powder was grinding the sample of the IOPCs to destroy the 3D ordered structure.

## **2.6 Preparation of NaYF<sub>4</sub>:Yb, Tm/Er UCNCs and TiO<sub>2</sub> composite film**

OA coated NaYF<sub>4</sub>: Yb, Tm/Er UCNCs were dissolved in cyclohexane with a concentration of 0.5 mg/mL. After that the glass substrate with (or without) the TiO<sub>2</sub> IOPCs was dropped vertically into the cyclohexane solution and placed in an oven at 25 °C for over 2 hours. With the slow volatilization of cyclohexane, the NaYF<sub>4</sub>: Yb, Er UCNCs were laxly self-organized into the void space of TiO<sub>2</sub> IOPCs or deposited directly on the surface of the glass substrate, driven by the capillary force of the liquid in the evaporation process. Similarly, the water-soluble PEI-NaYF<sub>4</sub>: Yb, Tm NCs dissolved in the PBS and TiO<sub>2</sub> IOPCs templates in the PBS were placed in an oven at 25 °C for over 8 hours.

## 2.7 Characterization.

The surface morphology of the as-prepared products were measured with a JEOL JSM-7500 field emission scanning electron microscope (FE-SEM) at an accelerating voltage of 15 kV. Transmission electron micrographs were carried out with a Hitachi H-800 transmission electron microscope (TEM) operating at an acceleration voltage of 200kV. The crystalline structure of the samples was characterized by X-ray diffraction (XRD) (Rigaku D/max-rA power diffractometer using Cu KR radiation ( $\lambda$ ) 1.54178 Å). Ultraviolet-visible (UV-Vis) absorption spectra were measured with a Shimadzu UV-3101PC UV-vis scanning spectrophotometer ranging of 200-1100nm.

## 2.8 Luminescence Measurement

The emission and excitation spectra of FITC and the composite films were measured with a SENS-9000 spectrometer. In the measurement of UCL spectra and dynamics of the composite films, a photomultiplier combined with a monochromator was used for signal collection from 300 nm to 750nm. A continuous 980 nm diode laser was used to pump the samples to investigate the steady-state spectra. In the measurements of luminescent dynamics and excitation wavelength-dependent UC enhancement, the samples were pumped by a laser-system consisting of a Nd:YAG pumping laser (1064-nm), the third-order Harmonic-Generator (355-nm) and a tunable optical parameter oscillator (OPO, Continuum Precision II 8000). It was with the pulse duration of 10 ns, repetition frequency of 10 Hz and line width of 4-7  $\text{cm}^{-1}$ .

## 3. Results and Discussion

### 3.1 Morphology and structure of NaYF<sub>4</sub>/TiO<sub>2</sub> composite films

The  $\text{NaYF}_4:\text{Yb}^{3+}, \text{Tm}^{3+}$  NCs with different sizes were synthesized by a solvothermal method referred in the part of the experiment section, and the  $\text{TiO}_2$  IOPCs were fabricated by a simple PMMA template removal method. The solvent evaporation method was used to assemble  $\text{NaYF}_4:\text{Yb}^{3+}, \text{Tm}^{3+}$  NCs layer-by-layer on the  $\text{TiO}_2$  film on a glass substrate. The preparation process was shown in the Scheme 1(a). Figure 1 (a)-(e) show the TEM images of the  $\text{NaYF}_4:\text{Yb}^{3+}, \text{Tm}^{3+}$  NCs prepared under different temperatures ( $280^\circ\text{C}$ ,  $290^\circ\text{C}$ ,  $300^\circ\text{C}$ ,  $320^\circ\text{C}$  and  $330^\circ\text{C}$ ). It can be distinguished that all the NCs are single-dispersed and homogeneous. The average sizes of  $\text{NaYF}_4:\text{Yb}^{3+}, \text{Tm}^{3+}$  NCs increase with the increasing reacting temperature, and they are determined to be 5, 7, 25, 35 and 50 nm, respectively, for the samples prepared at 280, 290, 300, 320 and  $330^\circ\text{C}$ . Figure 1(f) shows the XRD of the as-prepared NCs and the standard cards of the  $\alpha$ - $\text{NaYF}_4$ ,  $\beta$ - $\text{NaYF}_4$  as control. As can be seen, the products prepared under  $280^\circ\text{C}$  and  $290^\circ\text{C}$  are cubic in phase, and when the temperature increases to  $300^\circ\text{C}$ , the NCs transfer to hexagonal phase. On further increasing the temperature, the  $\text{NaYF}_4$  is still hexagonal in phase without other impurity peaks. Figure 2(a) shows the SEM image of the  $\text{TiO}_2$  IOPCs. It can be seen that the sample is long-range ordered hexagonal arrangement of inverse opal with the center-to-center distance of  $\sim 420$  nm. For the structure of the composite films, we took the 35 nm  $\text{NaYF}_4:\text{Yb}^{3+}, \text{Tm}^{3+}$  NCs/ $\text{TiO}_2$  IOPCs composite film for example. From the top view of the composite film (seeing Figure 2(b)), it can be seen that after loading the  $\text{NaYF}_4:\text{Yb}^{3+}, \text{Tm}^{3+}$  NCs, the interspaces of  $\text{TiO}_2$  IOPCs are occupied by NCs, as well as the structure of the  $\text{TiO}_2$  IOPCs is not destroyed by the cyclohexane.

Figure 2(c) indicates that continuous  $\text{NaYF}_4:\text{Yb}^{3+}, \text{Tm}^{3+}$  films are formed on the glass substrate, consisting of closely packed NCs. To determine the relative thickness of the NCs on the film and the glass, we measured the transmission of NCs on the glass, and the composite film as  $T_1, T_2$ . In measurement of  $T_1, T_2$ , the glass and the  $\text{TiO}_2$  IOPCs were used as reference samples, respectively. According to the Beer-Lambert Law, the relationship of the transmission and the absorption can be written as

$$A_i = \lg(1/T_i), i = 1, 2 \quad (1)$$

where the  $A_i$  and  $T_i$ , respectively, stand for value of absorbance and transmittance for the  $\text{NaYF}_4:\text{Yb}^{3+}, \text{Tm}^{3+}/\text{Er}^{3+}$  film ( $i=1$ ) and the composite film ( $i=2$ ). Then we could get  $A_1, A_2$ . The absorbance ( $A_i$ ) is linearly related with the thickness of the film ( $D_i$ ), so by the measurement of  $T_i$ , the relative thickness of  $\text{NaYF}_4$  in different samples can be obtained, as listed in Table 1. It can be observed that with the increase of  $\text{NaYF}_4$  particle size, the relative thickness of the  $\text{NaYF}_4$  thin film and the  $\text{NaYF}_4/\text{TiO}_2$  film hybrid gradually increases. In comparison to the  $\text{NaYF}_4$  thin film on the glass, the  $\text{NaYF}_4$  layer grown on the  $\text{TiO}_2$  IOPC becomes a little bit thicker. It should be noted that in the following experiments on EF of UCL, the influence of thickness of  $\text{NaYF}_4$  has been considered. Figure 2(d) depicts the XRD patterns of the  $\text{TiO}_2$  IOPCs, the  $\text{TiO}_2$  powder and the composite film in contrast of the standard card, it can be seen that the samples are exactly corresponding with the standard card (JPCDS: 84-1285). No impurity peak appears, indicating that the samples are anatase in phase, moreover, some of peaks of the IOPCs are too weak to display because of the diffraction of the glass substrate. The XRD pattern of the composite film exhibited the diffraction peaks

of NaYF<sub>4</sub> in cubic phase (marked with asterisks \*) besides the TiO<sub>2</sub> diffraction peaks. According to the width of the XRD patterns and Scherrer formula, the nanocrystalline size of TiO<sub>2</sub> NCs consisting of the layer can be determined, to be ~16.4 nm.

### 3.2 UCL enhancement of the NaYF<sub>4</sub>/TiO<sub>2</sub> composite film and its mechanism

In this work, the UCL of the NCs was measured by the transmission method, and the optical circuit was shown in scheme 1(b). All the samples were measured and compared under the excitation of a 980-nm laser diode with the same excitation power density (48 mW/mm<sup>2</sup>), and in the measurements the optical circuit remained unchanged. Figure 3 shows the comparison of UCL spectra under 980-nm excitation between the 5-nm-NaYF<sub>4</sub>:Yb<sup>3+</sup>, Tm<sup>3+</sup> NCs deposited directly on the glass substrate and the 5-nm-NaYF<sub>4</sub>:Yb<sup>3+</sup>, Tm<sup>3+</sup> NCs deposited on the TiO<sub>2</sub> IOPCs. A number of UC emission lines can be observed for both the two samples, extending from the near ultraviolet to near-infrared region. The two lines in the near ultraviolet region are assigned to <sup>1</sup>I<sub>6</sub>-<sup>3</sup>F<sub>4</sub>(354nm) and <sup>1</sup>D<sub>2</sub>-<sup>3</sup>H<sub>6</sub> (367nm) of Tm<sup>3+</sup>, the lines in the blue region are derived from <sup>1</sup>D<sub>2</sub>-<sup>3</sup>F<sub>4</sub> (457nm) and <sup>1</sup>G<sub>4</sub>-<sup>3</sup>H<sub>6</sub> (484nm) transitions, and the lines within the red to infrared region are attributed to the transitions of <sup>1</sup>G<sub>4</sub>-<sup>3</sup>F<sub>4</sub> (653 nm) and <sup>3</sup>F<sub>2</sub>-<sup>3</sup>H<sub>6</sub>(703nm), <sup>3</sup>F<sub>3</sub>-<sup>3</sup>H<sub>6</sub>(731nm). The inset of Figure 3 shows the schematic of UC populating and emission processes of NaYF<sub>4</sub>: Tm<sup>3+</sup>, Yb<sup>3+</sup> under the excitation of the 980 nm laser diode.<sup>29</sup> Based on the inset of Figure 3, the populations on <sup>1</sup>I<sub>6</sub>, <sup>1</sup>D<sub>2</sub>, <sup>1</sup>G<sub>4</sub> originate from a five-photon process, a four-photon process, and a three-photon process, respectively, while, the populations on <sup>3</sup>F<sub>2</sub>, and <sup>3</sup>F<sub>3</sub> are both from a two-photon process. In contrast to the 5-nm-NaYF<sub>4</sub>:Yb<sup>3+</sup>, Tm<sup>3+</sup> NCs thin film on the

glass, the overall UCL intensity in the composite film increases by more than 43-fold.

To determine the mechanism of UC enhancement, we first measured the UCL spectra under the excitation of 980-nm laser with different powers on the sample of 35-nm NaYF<sub>4</sub>:Yb<sup>3+</sup>, Tm<sup>3+</sup> NCs/ TiO<sub>2</sub> IOPCs composite film and the corresponding NC film. It should be noted that the EFs we mentioned in this paper are all corrected by the relative thickness, which can be expressed as,

$$EF = \frac{I_2}{I_1} \times \frac{D_1}{D_2}, \quad (2)$$

where  $I_i$  and  $D_i$  stand for the intensity and the thickness of the samples, respectively.

Figure 4(a) shows the dependence of EF on different UC transitions (<sup>1</sup>I<sub>6</sub>-<sup>3</sup>F<sub>4</sub>, <sup>1</sup>D<sub>2</sub>-<sup>3</sup>H<sub>6</sub>+<sup>1</sup>D<sub>2</sub>-<sup>3</sup>F<sub>4</sub>, and <sup>1</sup>G<sub>4</sub>-<sup>3</sup>H<sub>6</sub>+<sup>1</sup>G<sub>4</sub>-<sup>3</sup>F<sub>4</sub>) and excitation power. It can be seen that while the excitation power was fixed at a certain value, the higher the excited level was, the larger the EF under the same excitation power was. This definitely reveals that the UC enhancement is probably associated with the enhancement of the excitation light due to the modulation of PCs. It can be also seen that for all the transitions, EF gradually decreased with the increase of excitation power. EF of the overall integrated intensity from 300 nm to 750 nm gradually decreased from 17-fold to 6-fold as the power of excitation increased from 0.09W to 0.93W. This phenomenon was also observed in the dense composite film of silver/NaYF<sub>4</sub>:Yb<sup>3+</sup>,Er<sup>3+</sup> and was attributed to the local thermal effect induced by the irradiation of laser diode.<sup>25</sup> As is well known, the intensity ratio ( $R_{HS}$ ) of <sup>3</sup>F<sub>2</sub>-<sup>3</sup>H<sub>6</sub> to <sup>3</sup>F<sub>3</sub>-<sup>3</sup>H<sub>6</sub> is sensitive to temperature and is a critical parameter to determine the temperature change in UCL processes due to energy gap of <sup>3</sup>F<sub>3</sub> and <sup>3</sup>F<sub>2</sub>. According to the Boltzmann's distribution and the value of  $R_{HS}$ , the

local temperature as a function of excitation power of the samples can be deduced, as shown in Fig.4 (b). It is obvious that while under the identical excitation power, the temperature of the NaYF<sub>4</sub>:Yb<sup>3+</sup>, Tm<sup>3+</sup>/TiO<sub>2</sub> composite film increases much higher than that of the NaYF<sub>4</sub>:Yb<sup>3+</sup>, Tm<sup>3+</sup> film. The improvement of local thermal temperature in the composite film would induce thermal quenching of the UCL, resulting in the decrease of EF with the increasing excitation power.

The UCL integrated intensity of the transitions of <sup>1</sup>G<sub>4</sub>-<sup>3</sup>H<sub>6</sub>, <sup>1</sup>D<sub>2</sub>-<sup>3</sup>F<sub>4</sub>, and <sup>1</sup>I<sub>6</sub>-<sup>3</sup>F<sub>4</sub> as a function of excitation power was also recorded and the ln–ln plots were shown in Fig. 4(c)-4(e), respectively. Generally, for UC, the UCL intensity ( $I_{UCL}$ ) is proportional to the infrared excitation power ( $I_P$ ):  $I_{UCL} \propto I_P^n$  where  $n$  is the number of IR photons absorbed per visible photon emitted.<sup>30</sup> In Fig. 4(c)-4(e) for the NaYF<sub>4</sub>:Yb<sup>3+</sup>, Tm<sup>3+</sup> thin film the slopes  $n$  of the UCL are  $n=1.79$  for three-photon <sup>1</sup>G<sub>4</sub>-<sup>3</sup>H<sub>6</sub>,  $n=2.17$  for four-photon <sup>1</sup>D<sub>2</sub>-<sup>3</sup>F<sub>4</sub>, and  $n=2.64$  for five <sup>1</sup>I<sub>6</sub>-<sup>3</sup>F<sub>4</sub>. The slopes  $n$  for the NaYF<sub>4</sub>:Yb<sup>3+</sup>, Tm<sup>3+</sup>/TiO<sub>2</sub> IOPCs composite film are slightly lower ( $n=1.31$  for <sup>1</sup>G<sub>4</sub>-<sup>3</sup>H<sub>6</sub>,  $n=1.44$  for <sup>1</sup>D<sub>2</sub>-<sup>3</sup>F<sub>4</sub>, and  $n=1.77$  for <sup>1</sup>I<sub>6</sub>-<sup>3</sup>F<sub>4</sub>). For any multi-photon process, the slope  $n$  is approximately equal to photon number in general case, nevertheless, the values of  $n$  are all much smaller than the required photon numbers to populate the corresponding excited levels, which can be attributed to saturation effects of the UC processes.<sup>31</sup> The saturation effect, which causes  $n$  to deviate from the theoretical photon number, depending on the competition between linear decay and UC processes for the depletion of the intermediate excited states. If the linear decay is dominant, the slope will be close to the theoretical value, whereas if the UC is dominant, the slope will be

lower than the theoretical value. Therefore, the decrease of slope  $n$  in the composite film indicates that the saturation effect happens more easily than that in the NaYF<sub>4</sub> film due to the modulation of TiO<sub>2</sub> IOPCs. It is suggested that the structure of the TiO<sub>2</sub> IOPCs allows the enhanced scattering of the 980-nm laser, which equals to enhance the excitation power for the composite film and more conducive to the UC process, leading to the increased saturation effect.

Furthermore, we measured the size-dependence and photonic stop band (PSB)-dependence of the UCL intensity of NaYF<sub>4</sub>:Yb<sup>3+</sup>, Tm<sup>3+</sup> thin film and NaYF<sub>4</sub>:Yb<sup>3+</sup>, Tm<sup>3+</sup> NCs/ TiO<sub>2</sub> IOPCs composite film on the same conditions. The EF versus the particle size of NaYF<sub>4</sub>:Yb<sup>3+</sup>, Tm<sup>3+</sup> NCs in composite film is shown in the Figure 5(a). Note that the UCNCs with different sizes were all composited on the TiO<sub>2</sub> IOPCs with the PSB of 650 nm. As can be seen, EF increases remarkably with the decreasing particle size of NaYF<sub>4</sub> on the composite film. As the particle size decreases from 50 nm to 5 nm, EF gradually increases from 3 folds to 43 folds. As described in the above section, the thickness of the NaYF<sub>4</sub> layer for the 50-nm NaYF<sub>4</sub>/TiO<sub>2</sub> composite film is 3.8-fold compared to the 50-nm NaYF<sub>4</sub>/TiO<sub>2</sub> composite film (see Table 1). More excitation laser should be absorbed by the NaYF<sub>4</sub> layer when it passes through the thicker film. As a consequence, the residual light being scattered by the IOPCs reduces, resulting in the decrease of EF with the increase of NaYF<sub>4</sub> particle size. In our previous work, we fabricated the porous structure of the silver film/NaYF<sub>4</sub>:Yb<sup>3+</sup>, Er<sup>3+</sup> composite and observed similar size-dependent UC enhancement. It was mainly attributed to the decrease in the

interaction distance between the surface plasmon of silver and the UCNCs.<sup>25</sup>

Fig. 5(b) shows the dependence of the overall EF as a function of PSB location. The IOPCs with different PSBs were all composited with the 5-nm-NaYF<sub>4</sub>:Yb<sup>3+</sup>, Tm<sup>3+</sup> NCs. The inset shows the transmittance spectra of various TiO<sub>2</sub> IOPCs, which indicates that the PSB can be tuned in the range of 400-1000 nm, which is allowed to overlap with the emission and excitation lines of Tm<sup>3+</sup>. However, the depth of the PSB is shallow, ranging of only 2-3 % in transmittance. It is apparent that as the PSB changes, the EF changes randomly in the range of 39 to 47, regardless of whether the PSB is overlapping with the emission field or the excitation field of Tm<sup>3+</sup>. In our previous work, we studied the coupling of PMMA opal PCs with deep PSB (more than 50% in transmittance) to NaYF<sub>4</sub>:Yb<sup>3+</sup>, Tm<sup>3+</sup> composite film and observed EF depended strongly on PSB. An optimum was obtained as its PSB was tuned to ~980 nm, exactly overlapping with the excitation light.<sup>24</sup> In the present case, because the shallow PSB of the TiO<sub>2</sub> IOPCs, the PSB effect is not obvious. The UC enhancement could be mainly attributed to random diffraction of the TiO<sub>2</sub> multi-layer structure to the excitation light.

In order to further understand the mechanism of the UC enhancement, the UCL dynamic processes of the excited states <sup>1</sup>G<sub>4</sub>-<sup>3</sup>H<sub>6</sub> for Tm<sup>3+</sup> ions in different samples were measured at the room temperature. All the dynamical curves exhibit the same trends, namely, after an initial rise; the intensity of luminescence reaches a maximum and then decays following an exponential process. The curves can be well fitted by the following equation<sup>32</sup>:

$$I(t) = I_D e^{-t/\tau_D} - I_R e^{-t/\tau_R}, \quad (3)$$

where  $\tau_D$  and  $\tau_R$  represent the exponential decay and rising time constants, respectively, and  $I_D$ ,  $I_R$  are both the positive constants. It should be highlighted that  $\tau_D$  is dominated by the depopulation of electrons on the emitting level, which mainly depends on the radiative and non-radiative transition rates of the  $^1G_4$  level for  $Tm^{3+}$  ions, while  $\tau_R$  is dominated by the population complement on  $^1G_4$ , which strongly depends on the ET rate from  $Yb^{3+}$  to the  $^1G_4$  level.

Fig. 6 demonstrates the rising and the decay time constants of the  $^1G_4$ - $^3H_6$  for  $Tm^{3+}$  ions under the 980-nm laser in the thin film samples prepared with different  $NaYF_4$  NCs. It can be clearly distinguished that as the size of the  $NaYF_4$  NCs decreases from 50 nm to 5 nm,  $\tau_D$  and  $\tau_R$  both gradually decrease. This can be ascribed to the increase of large vibrational modes such as -OH involved on the surface of the NCs and their contribution to the nonradiative transitions.<sup>33</sup> Figure 6 also demonstrates that  $\tau_R$  and  $\tau_D$  for the composite film rarely change in comparison to those for the pure  $NaYF_4$  film. This suggests that the existence of  $TiO_2$  IOPCs layer in the composites do not change the radiative and nonradiative transition rates of the  $^1G_4$  and the other emission levels for  $Tm^{3+}$ . Based on all the facts above, we can conclude that the UC enhancement in  $NaYF_4/TiO_2$  composites is mainly due to the scattering of  $TiO_2$  IOPCs layer by layer to the incident excitation light of 980 nm.

Note that we also fabricated 5-nm- $NaYF_4:Yb^{3+}$ ,  $Er^{3+}/TiO_2$  composite film and the EF of overall UCL intensity (integrated from 300 to 750 nm) was 41-fold compared with the pure 5-nm- $NaYF_4:Yb^{3+}$ ,  $Er^{3+}$  film, which was similar to the case of

NaYF<sub>4</sub>:Yb,Tm. It is also important to point out that in the NaYF<sub>4</sub>/TiO<sub>2</sub> composite the remarkable visible enhancement for Er<sup>3+</sup> or Tm<sup>3+</sup> not only can be obtained under the excitation of infrared laser, but also can be also obtained under the excitation of visible lights, on the condition of downconversion (DC) luminescence and photoluminescence. Fig.7(a) shows the EF factor of Er<sup>3+</sup> photoluminescence under the excitation of lights with different wavelengths in 5-nm-NaYF<sub>4</sub>:Yb<sup>3+</sup>, Er<sup>3+</sup>/TiO<sub>2</sub> composite film(PSB~650nm). The dependence of EF on excitation wavelength ranging of 440-500 nm is for <sup>4</sup>S<sub>3/2</sub>-<sup>4</sup>I<sub>15/2</sub> transition, and ranging of 500-540 nm is for <sup>4</sup>F<sub>9/2</sub>-<sup>4</sup>I<sub>15/2</sub> transition. It can be observed that the average EF is 4.7 under the excitation wavelength of 440–450 nm, 7.5 of 480-490 nm and 14.3 of 500–540 nm. It is very interesting to observe that EF depends strongly on the wavelength of excitation light. The longer the excitation wavelength is, the larger the EF is. This fact can be well understood from the reflection spectra of the TiO<sub>2</sub> IOPCs with different PSBs, as shown in Fig7 (b). It can be observed that the narrower reflection of PSBs can be observed besides the sample with PSB of 980nm, and the reflection strength of PSB varies randomly. Besides the contribution of PSB, totally to say, the reflectance gradually increases with the increasing wavelength, for all the samples. Because the UC enhancement is induced by the scattering of TiO<sub>2</sub> IOPCs to the excitation light and roughly to say, the diffraction/reflection of the TiO<sub>2</sub> IOPCs increases with the increasing wavelength, thus EF increases with the increasing wavelength. It should be highlighted that the EFs under visible excitation are much smaller than that under 980-nm excitation, which can be attributed to the following two reasons. First, the

diffraction/reflection increases with the increase of wavelength. Second, for visible excitation, the emissions for  $\text{Er}^{3+}$  originate from one-photon process, while for 980-nm excitation, the emissions for the transitions of  $^4\text{S}_{3/2}-^4\text{I}_{15/2}$  and  $^4\text{F}_{9/2}-^4\text{I}_{15/2}$  both come from a two-photon, in which UCL is generally proportional to the square of excitation power.<sup>34</sup>

### 3.3 Detection of avidin with $\text{NaYF}_4:\text{Yb}^{3+},\text{Er}^{3+}/\text{TiO}_2$ IOPCs composite films

The solid-state bio-sensor based on UCNCs is desirable, which is very convenient for the detection and can be easily operated. However, it is difficult to be realized due to the confliction of larger surface area and smaller particle size of UCNCs with stronger UCL. In the present work, the composite films consisting of smaller  $\text{NaYF}_4$  UCNCs and  $\text{TiO}_2$  IOPCs which can largely enhance the UCL of smaller UCNCs are promised to overcome above problems.

For biodetection application, the NCs must be hydrophilic, the NCs we prepared before were synthesised in OA and ODE, which were hydrophobic organic solvents and are not water-soluble due to the lack of hydrophilic functional groups on their surfaces. Typically, additional surface-modification steps are required to link appropriate functional groups (e.g.  $\text{COOH}$ ,  $\text{NH}_2$ , or  $\text{SH}$ ) to obtain a hydrophilic surface for further conjugation of biomolecules.<sup>35,36</sup> The complicated procedures may affect the morphology and PL intensity of NCs, and this is disadvantage for potential applications of biodetection.<sup>20</sup> Considering of these points, in the biodetection part we developed one-step solvothermal route to prepare amine-functionalized  $\text{NaYF}_4:\text{Yb}/\text{Tm}$  NCs with PEI as surfactant that anchors on the surface of the NCs for

subsequent conjugation with biomolecule.

Amine-functionalized NaYF<sub>4</sub>:Yb, Tm NCs with PEI as capping agent to control the growth of NCs and to render them water-soluble and surface-functionalized. The amine groups on the surface of PEI- NaYF<sub>4</sub>:Yb, Tm NCs can link with carboxyl group of biotin (Scheme 2(a)). In addition, biotin have highly specific interaction with avidin, which have been widely applied in modern biological and medical fields.<sup>37-39</sup> The TEM images of as prepared water-soluble PEI-NaYF<sub>4</sub>: Yb, Tm UCNCs and biotinylation PEI-NaYF<sub>4</sub>: Yb, Tm NCs are shown in Figure 8(a) and 8(b), respectively. It can be seen that the NCs displayed in Fig. 8(a) and 8(b) are both uniform in size and morphology and are well-dispersed, and the average sizes of the NCs are both ~18 nm. This indicates that biotinylation of PEI-NaYF<sub>4</sub>: Yb, Tm UCNCs has no obvious adverse effect on the morphology. Fig. 8(c) exhibited the XRD patterns of the water-soluble PEI-NaYF<sub>4</sub>: Yb, Tm UCNCs and biotinylation PEI-NaYF<sub>4</sub>: Yb, Tm UCNCs. It can be seen that the samples are both in cubic phase before and after modified with biotin.

To verify the conjugation between PEI-NaYF<sub>4</sub>:Yb, Tm UCNCs and biotin, the as-prepared UCNCs before and after reaction were analyzed by FTIR spectra, as shown in Figure 8(d). It can be seen that both the PEI-UCNCs and biotinylation NaYF<sub>4</sub>:Yb,Tm samples exhibit a broad band around 3441cm<sup>-1</sup>, corresponding to N-H stretching vibration. These amine groups can link with carboxyl group of biotin to make amido linkage. In the biotin-PEI-UCNCs, a strong transmission band in the region around 1543 cm<sup>-1</sup> and 1409 cm<sup>-1</sup> can be observed, which is assigned to the

internal vibration of amide bonds, indicating that the UCNCs are coated with biotin. It is worth pointing that the Biotin-PEI-NaYF<sub>4</sub>: Yb, Tm on the TiO<sub>2</sub> IOPCs can be also largely enhanced versus that on the glass and EF is determined to be 18.4 under the excitation of 48 mW/mm<sup>2</sup> 980 nm light.

The principle of FRET detection of avidin by employing biotinylated NCs as energy donor and FITC-labeled avidin as energy acceptor is illustrated in Scheme 2(b). Excitation of biotinylated NaYF<sub>4</sub>:Yb<sup>3+</sup>,Tm<sup>3+</sup> NCs triggers energy transfer(ET) from Tm<sup>3+</sup> to FITC within a given proximity through specific binding between biotin and avidin, and results in emission from FITC at its characteristic wavelength. Here FITC was selected as an energy acceptor to couple with the NCs, because it has a broad excitation band centering at 490 nm which can well overlap the <sup>1</sup>G<sub>4</sub>-<sup>3</sup>H<sub>6</sub> emission lines of Tm<sup>3+</sup> peaking at 484 nm (see Figure 9a).

As shown in Figure 9(b), upon excitation of NCs under 980 nm laser diode, the emission band of FITC centered at 520 nm (referred as FITC<sub>520</sub> here after) gradually increases with the increasing amount of avidin, accompanying by the expense of <sup>1</sup>G<sub>4</sub>-<sup>3</sup>H<sub>6</sub> emission band of Tm<sup>3+</sup> centered at 480 nm (referred as Tm<sub>480</sub> here after). In order to confirm the occurrence of FRET and the specific reaction between the avidin and biotin, nonbinding control experiments were performed by employing the as-prepared NCs instead of the biotinylated NCs as bioprobes under otherwise identical conditions. No obvious enhancement of FITC emission with increasing the amount of FITC in the control group can be distinguished (see Figure 9(c)). This means that non-biotinylated NCs and FITC are far apart, and thus no FRET occur in

the control experiments. So, we can confirm that the specific interaction between biotin and avidin plays a key role to ensure proximity between the acceptor and the donor.

The left part of Figure 9(d) shows the curve of FITC<sub>520</sub>/Tm<sub>480</sub> as a function of the amount of avidin measured on the composite films. The signal of FITC<sub>520</sub>/Tm<sub>480</sub> increases steadily with the increasing of the avidin concentration. There has a good linear relationship and a high sensitivity between fluorescent intensity ratio and the concentration of avidin, R, defined as the correlation coefficient of the linear fit, is 0.996, the sensitivity is 34 pmol<sup>-1</sup>, when the concentration range is of 0-4.5nmol. The limit of detection (LOD) is 48 pmol, according to 3s/m, where m is the slope for the range of the linearity used and s is the standard deviation.<sup>40</sup> Note that Chen reported the time-resolved DC-FRET biosensor based on amine-functionalized NaYF<sub>4</sub>: Ce, Tb nanocrystals with a detection limit of about 5 nM.<sup>41</sup> Additionally, the LOD of the previous results based on UC-FRET employing Y<sub>2</sub>O<sub>2</sub>S:Er/Yb as donor and phycobiliprotein as acceptor is 0.7–9.0 nM.<sup>42</sup>

Another control experiment was implemented by the PBS solution containing of NCs instead of the composite films as the biosensor under otherwise identical conditions. The right part of Figure 9(d) shows that the variation trend of the signal of FITC<sub>520</sub>/Tm<sub>480</sub> is same as that measured on the composite film, however, the linear relationship is not very good, when the range is of 0-4.5nmol, R is fitted as 0.979, the sensitivity is 27 pmol<sup>-1</sup>, however, the LOD of the liquid sensor is 110 pmol. The facts indicate that the UCL of NCs on the composite film is more stable and sensitive than

that in the solution; meanwhile, the sensitivity of the solid-sensor is much better than the liquid-based sensor.

To further confirm the FRET process, we measured the UCL dynamic process. Figure 10(a) shows the UCL dynamic curves of transition of  ${}^1G_4-{}^3H_6$  of  $Tm^{3+}$  under excitation of 980-nm with the different adding amount of avidin, which can be well fitted to a double exponential function described by Eq.3. The constants of the rising and decay time as a function of the amount of avidin were shown in Fig. 10(b). It can be clearly seen that the decay time reduces from 197 to 131 $\mu$ s with the increasing concentration of avidin from 0 to 4.5nmol. However, the rising time is almost unchanged with the variation of the concentration. This is another unambiguously evidence for the occurrence of FRET from  $Tm^{3+}$  to FITC. The decay lifetime of the energy donor, which is hardly affected by environmental factors such as re-absorption and the concentration of NCs, may provide another important parameter to measure the ET efficiency in FRET bioassays.

For an excellent biosensor, high photostability is very important. Therefore, the photostability of UC composite film under illumination of 980 nm light were investigated. Meanwhile, we took DC composite film (biotin-PEI-NaYF<sub>4</sub>: 5% Ce, 5% Tb) under illumination of 290 nm light by comparison. After adding the same amount of the avidin-FITC, the films excited under continuous illumination using a 980 nm laser or 290 nm lamp for 1h. From Figure 11 it can be seen that the emission intensity of FITC of DC composite film decreased to 73% after illumination for 1h, while the intensity of FITC of UC composite film was steady under 1h excitation. The UC film

exhibiting excellent photostability is more useful in practical applications. The inset of Fig. 11 shows the emission spectra of the films added with avidin-FITC under excitation of 980 nm laser or 290 nm lamp.

#### 4. Conclusions

In this work, we fabricated some novel composite films,  $\text{NaYF}_4:\text{Yb}^{3+},\text{Tm}^{3+}(\text{Er}^{3+})/\text{TiO}_2$  IOPCs by the self-assemble technique. By the modulation of  $\text{TiO}_2$  IOPCs, highly enhanced emissions of  $\text{Tm}^{3+}/\text{Er}^{3+}$  were observed in the composite films under anti-Stokes 980-nm excitation as well as visible Stokes excitation. It is interesting to observe that the EF, depends strongly on excited energy levels of  $\text{Tm}^{3+}/\text{Er}^{3+}$ , excitation power of laser diode, particle size of  $\text{NaYF}_4:\text{Yb}^{3+},\text{Tm}^{3+}(\text{Er}^{3+})$  NCs for anti-Stokes 980-nm excitation and the wavelength of excitation light for visible Stokes excitation, while the EF is nearly independent of PSB. An optimum EF of 43-fold was obtained for the UCL of 5-nm- $\text{NaYF}_4:\text{Yb}^{3+}, \text{Tm}^{3+}$  NCs composite film with this strategy. As to the enhancement mechanism, was mainly attributed to the random diffraction of IOPCs multi-layers to the excitation light. Moreover, based on this unique structure, specific interaction between biotin and avidin, and FRET between Tm and FITC, the UC composite film was used for detecting avidin. The system offers two parameters for detection, namely, the emission intensity and the fluorescent decay time. As a FRET solid biosensor, the sensor can efficiently detects trace amount of avidin with a lot of advantages such as convenient detecting, good linear relationship ( $R=0.996$ ), low detection limit (48pmol), high sensitivity (34  $\text{pmol}^{-1}$ ), and photostability, and thus may have great potential for versatile

applications in biodetection.

## Acknowledgments

This work was supported by the Major State Basic Research Development Program of China (973 Program) (No. 2014CB643506), the National Natural Science Foundation of China (Grant no. 11374127, 11304118, 61204015, 81201738, 81301289, 61177042, and 11174111), Program for Chang Jiang Scholars and Innovative Research Team in University (No. IRT13018). The China Postdoctoral Science Foundation Funded Project (2012M511337 and 2013T60327), and the State Key Laboratory of Bioelectronics of Southeast University.

## References

- 1 F. Auze, *Chem. Rev.*, 2004, **104**, 139.
- 2 M. Haase, H. Schafer, *Angew. Chem. Int. Ed.*, 2011, **50**, 5808.
- 3 D. K. Chatterjee, A. J. Rufaihaha, Y. Zhang, *Biomaterials*, 2008, **29**, 937.
- 4 W.Q. Zou, C. Visser, J. A. Maduro, M. S.Pshenichnikov, J. C. Hummelen, *Nat. Photonics*, 2012, **6**, 560.
- 5 H. Lin, G. Meredith, S. B. Jiang, *J. Appl. Phys.*, 2003, **93**, 186.
- 6 R. D. Maio, B. Kokuoz, J. Ballato, *Opt. Express*, 2006, **14**, 11412.
- 7 J. Zhou, Z. Liu, F. Y. Li, *Chem. Soc. Rev.*, 2012, **41**, 1323.
- 8 F. Wang, X.G Liu, *Chem. Soc. Rev.*, 2009, **38**, 976.
- 9 F. Vetrone, R. Naccache, A. Zamarro'n, A. J. Fuente, F.S. Rodriguez, L. M. Maestro, E. M. Rodriguez, D. Jaque, J.G. Sole, J. A. Capobianco, *ACS Nano*, 2010, **4**, 3254.
- 10 Y. H. Chien, Y. L. Chou, S. W. Wang, S. T. Hung, M. C. Liau, Y. Chao, C. H. Su, C. S. Yeh, *ACS Nano*, 2013, **7**, 8516.
- 11 L. N. Sun, H. S. Peng, M. I. J. Stich, D. Achatz, O. S. Wolfbeis, *Chem. Comm.*, 2009, 5000.
- 12 J. L. Liu, Y. Liu, Q. Liu, C. Y. Li, L. N. Sun, F. Y. Li, *J. Am. Chem. Soc.*, 2011, **133**, 15276.
- 13 Y. H. Wang, Z. J. Wu, Z. H. Liu, *Anal. Chem.*, 2013, **85**, 258.
- 14 Y. H. Wang, P. Shen, C. Y. Li, Y. Y. Wang, Z. H. Liu, *Anal. Chem.*, 2012, **84**, 1466.
- 15 J. Zhang, B. Li, L. M. Zhang, H. Jiang, *Chem. Comm.*, 2012, **48**, 4860.
- 16 R.R. Deng, X. J. Xie, M. Vendrell, Y. T. Chang, X. G. Liu, *J. Am. Chem. Soc.*, 2011,

- 133**, 20168.
- 17 Y. Liu, M. Chen, T. Y. Cao, Y. Sun, C. Y. Li, Q. Liu, T. Yang, L. M. Yao, W. Feng, F. Y. Li, *J. Am. Chem. Soc.*, 2013, **135**, 9869.
- 18 (a) Q. Liu, Y. Sun, T. S. Yang, W. Feng, C. G. Li, F. Y. Li, *J. Am. Chem. Soc.*, 2011, **133**, 17122. (b) Y. Sun, X. J. Zhu, J. J. Peng, F. Y. Li, *ACS Nano*, 2013, **7**, 11290.
- 19 (a) F. Wang, Y. Han, C. S. Lim, Y. H. Lu, J. Wang, J. Xu, H. Y. Chen, C. Zhang, M. H. Hong, X. G. Liu, *Nature*, 2010, **463**, 1061. (b) D. Q. Chen, Y. S. Wang, *Nanoscale*, 2013, **5**, 4621. (c) L. Lei, D. Q. Chen, P. Huang, J. Xu, R. Zhang, Y. S. Wang, *Nanoscale*, **5**, 11298.
- 20 G. S. Yi, G. M. Chow, *Chem. Mater.*, 2007, **19**, 341.
- 21 M. Saboktakin, X. C. Ye, S. J. Oh, S. H. Hong, A. T. Fafarman, U. K. Chettiar, N. Engheta, C. B. Murray, C. R. Kagan, *ACS Nano*, 2012, **6**, 8758.
- 22 H. P. Paudel, L. L. Zhong, K. Bayat, M. F. Baroughi, S. Smith, C. K. Lin, C. Y. Jiang, M. T. Berry, P. S. May, *J. Phys. Chem. C*, 2011, **115**, 19028.
- 23 P. Y. Yuan, Y. H. Lee, M. K. Gnanasammandhan, Z. P. Guan, Y. Zhang, Q. H. Xu, *Nanoscale*, 2012, **4**, 5132.
- 24 Z. Yin, Y. S. Zhu, W. Xu, J. Wang, S. Xu, B. Dong, L. Xu, S. Zhang, H. W. Song, *Chem. Commu.*, 2013, **49**, 3781.
- 25 W. Xu, Y. S. Zhu, X. Chen, J. Wang, L. Tao, S. Xu, T. Liu, H.W. Song, *Nano Res.*, 2013, **6**, 795.
- 26 Q.W. Li, G. A. Luo, J. Feng, Q. Zhou, L. Zhang, Y.F. Zhu, *Electroanal.*, 2001, **13**, 413.

- 27 Z. Q. Li, and Y. Zhang, *Nanotechnology*, 2008, **19**, 345606.
- 28 F. Wang, and X. G. Liu, *J. Am. Chem. Soc.*, 2008, **130**, 5642.
- 29 X. Bai, D. Li, Q. Liu, B. Dong, S. Xu, H.W. Song, *J. Mater. Chem.*, 2012, **22**, 24698.
- 30 M. Pollnau, D. R. Gamelin, S. R. Luthi, H. U. Gudel, *Phys. Rev. B*, 2000, **61**, 3337.
- 31 X. Bai, H. W. Song, G. H. Pan, Y. Q. Lei, T. Wang, X. G. Ren, S. Z. Lu, B. Dong, Q. L. Dai, L. B. Fan, *J. Phys. Chem. C*, 2007, **111**, 13611.
- 32 S. Xu, W. Xu, B. Dong, X. Bai, H.W. Song, *J. Appl. Phys.*, 2011, **110**, 113113.
- 33 Y. Wang, L. P. Tu, J. W. Zhao, Y. J. Sun, X. G. Kong, H. Zhang, *J. Phys. Chem. C*, 2009, **113**, 7164.
- 34 N. Liu, W. P. Qin, G. S. Qin, T. Jiang, D. Zhao, *Chem. Commun.*, 2011, **47**, 7671.
- 35 J. F. Jin, Y. J. Gu, C. W. Y. Man, J. P. Cheng, Z. H. Xu, Y. Zhang, H. S. Wang, H. Y. Lee, S. H. Cheng, W. T. Wong, *ACS Nano*, 2011, **5**, 7838.
- 36 R. Naccache, F. Vetrone, V. Mahalingam, Louis A. Cuccia, J. A. Capobianco, *Chem. Mater.*, 2009, **21**, 717.
- 37 Z.G. Chen, H.L. Chen, H. Hu, M.X. Yu, F.Y. Li, Q. Zhang, Z.G. Zhou, T. Yi, C.H. Huang, *J. Am. Chem. Soc.*, 2008, **130**, 3023.
- 38 K. K. Caswell, J. N. Wilson, U. H. F. Bunz, C. J. Murphy, *J. Am. Chem. Soc.*, 2003, **125**, 13914.
- 39 R. J. Pei, Z. L. Cheng, E.K. Wang, X. R. Yang, *Biosens. Bioelectron.*, 2001, **16**, 355.
- 40 Y. H. Wang, L. Bao, Z. H. Liu, D. W. Pang, *Anal. Chem.*, 2011, **83**, 8130.

41 D. T. Tu, L. Q. Liu, Q. Ju, Y. S. Liu, H. M. Zhu, R. F. Li, and X. Y. Chen , *Angew.*

*Chem. Int. Ed.*, 2011, **50**, 6306.

42 K. Kuningas, T. Rantanen, T. Ukonaho, T. Lo1vgren, T. Soukka, *Anal. Chem.*,

2005, **77**, 7348.

## Figure Captions

**Table 1** Relative thickness of the NaYF<sub>4</sub> layer prepared with different sizes of NaYF<sub>4</sub> UCNCs on the glass substrate ( $d_1$ ) and TiO<sub>2</sub> IOPCs ( $d_2$ ) and the ratio of  $d_2/d_1$ . Here the thick of the 5-nm NaYF<sub>4</sub> film was nomoalized.

**Scheme 1** (a) The formation of TiO<sub>2</sub> IOPCs/NaYF<sub>4</sub>:Yb,Tm UCNC composites, (b) The fluorescence measurement method.

**Shemem 2** (a) Biotinylation of PEI-capped NaYF<sub>4</sub>, and (b) FRET detection of avidin by employing biotinylated NCs as donor and FITC as acceptor.

**Figure 1** (a)–(e) TEM images of NaYF<sub>4</sub> samples prepared at different temperatures ranging from 280 to 330 °C. (f) XRD patterns of the as-prepared NaYF<sub>4</sub>:Yb, Er NCs fabricated at different temperatures with the standard cards for  $\alpha$ -NaYF<sub>4</sub> and  $\beta$ -NaYF<sub>4</sub>, for comparison.

**Figure 2** (a) SEM images of TiO<sub>2</sub> IOPCs, and (b) 35-nm-NaYF<sub>4</sub>:Yb, Er/TiO<sub>2</sub> composites, and (c) 35-nm-NaYF<sub>4</sub>:Yb, Er nanofilm deposited directly onto the glass substrate.(d) XRD patterns of TiO<sub>2</sub> IOPCs, the TiO<sub>2</sub> powder and the composite film in contrast of the standard card.

**Figure 3** A comparison of UCL spectra of 5-nm-NaYF<sub>4</sub>:Yb,Tm film and the 5-nm-NaYF<sub>4</sub>:Yb, Tm/TiO<sub>2</sub> composites, inset: UC population and emission processes of NaYF<sub>4</sub>:Yb, Tm UCNCs

**Figure 4** (a) Power-dependence of EF, (b) The deduced sample temperature based on  $R_{HS}$  of the NaYF<sub>4</sub>:Yb, Tm film and the NaYF<sub>4</sub>:Yb, Tm/TiO<sub>2</sub> composites. ln–ln plots of the (c)  $^1G_4$ - $^3H_6$ , (d)  $^1D_2$ - $^3F_4$ , (e)  $^1I_6$ - $^3F_4$  emission intensity

**Figure 5** (a) The size-dependence of UCL EF, (b) The dependence of the UC EF as a function of PSB of TiO<sub>2</sub> IOPCs

**Figure 6** The size-dependence of the UCL lifetimes including the rising and the decay time constants of the <sup>1</sup>G<sub>4</sub>-<sup>3</sup>H<sub>6</sub> transitions for Tm<sup>3+</sup> ions in the NaYF<sub>4</sub> film and the NaYF<sub>4</sub>:Yb, Tm/TiO<sub>2</sub> composites.

**Figure 7** (a) The excitation wavelength (ranging from 440–500 nm) dependence of EF for <sup>4</sup>S<sub>3/2</sub>-<sup>4</sup>I<sub>15/2</sub>, and the excitation wavelength (ranging from 500-540 nm) dependence of EF for <sup>4</sup>F<sub>9/2</sub>-<sup>4</sup>I<sub>15/2</sub> transition in the NaYF<sub>4</sub>: Yb, Er film and the NaYF<sub>4</sub>:Yb, Er/TiO<sub>2</sub> composites. (b) Reflection spectra of the IOPCs with different PSB

**Figure 8** (a)(b) TEM images of the as prepared water-soluble PEI-NaYF<sub>4</sub>: Yb, Tm UCNCs and biotinylation PEI-NaYF<sub>4</sub>: Yb, Tm UCNCs. (c) XRD patterns of the NaYF<sub>4</sub>:Yb,Tm UCNCs before and after modified with biotin in contrast of the standard card for α -NaYF<sub>4</sub>. (d) FTIR spectra of the NaYF<sub>4</sub>:Yb,Tm UCNPs before and after modified with biotin.

**Figure 9** (a) Emission (blue line) spectrum of biotinylated NCs; excitation (yellow dashed line) and emission (green solid line) spectra of FITC. (b) FRET spectra of bioassay experiments at different concentrations of avidin. (c) The red dots indicate the bioassay experiments in which FITC is FRET-sensitized by biotinylated NCs through the avidin–biotin interaction and the green dots show the control experiments with FITC and no amine-enriched NCs, for which no binding and hence no FRET occurs. (d) Calibration curve of FRET detection on the IOPC (left part) and in the

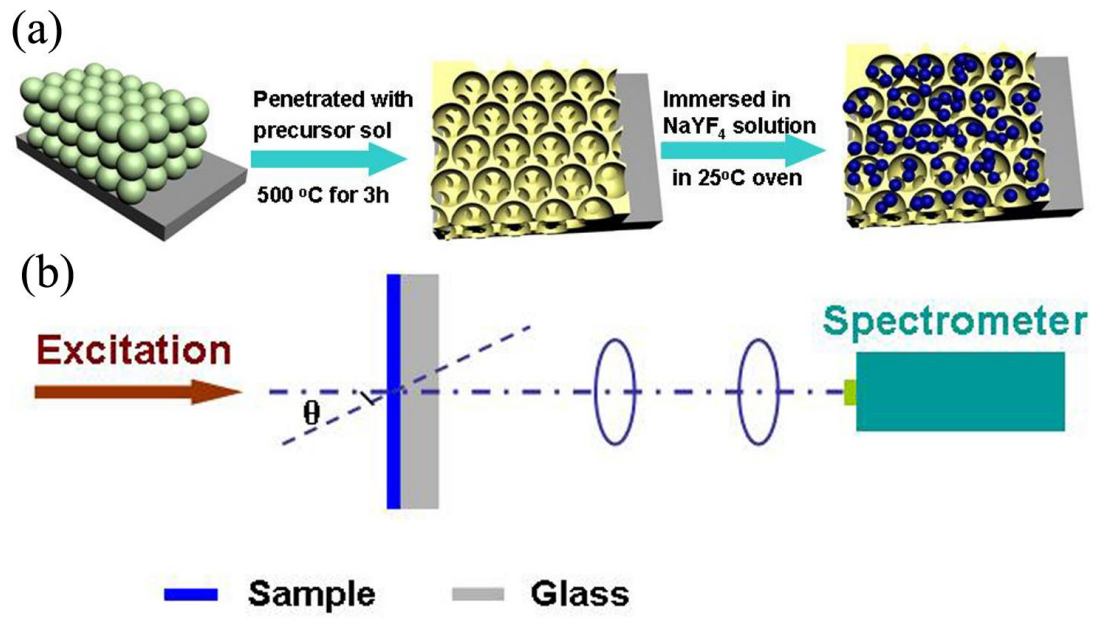
solution (right part) for the integrated PL intensity ratio  $\text{FITC}_{520}/\text{Tm}_{480}$  versus the concentration of avidin.

**Figure 10** (a) The curves of the  $^1\text{G}_4$  of  $\text{Tm}^{3+}$  at different concentrations of avidin. (b) Rising and decay lifetime constants of  $^1\text{G}_4$  of  $\text{Tm}^{3+}$  at different concentrations of avidin.

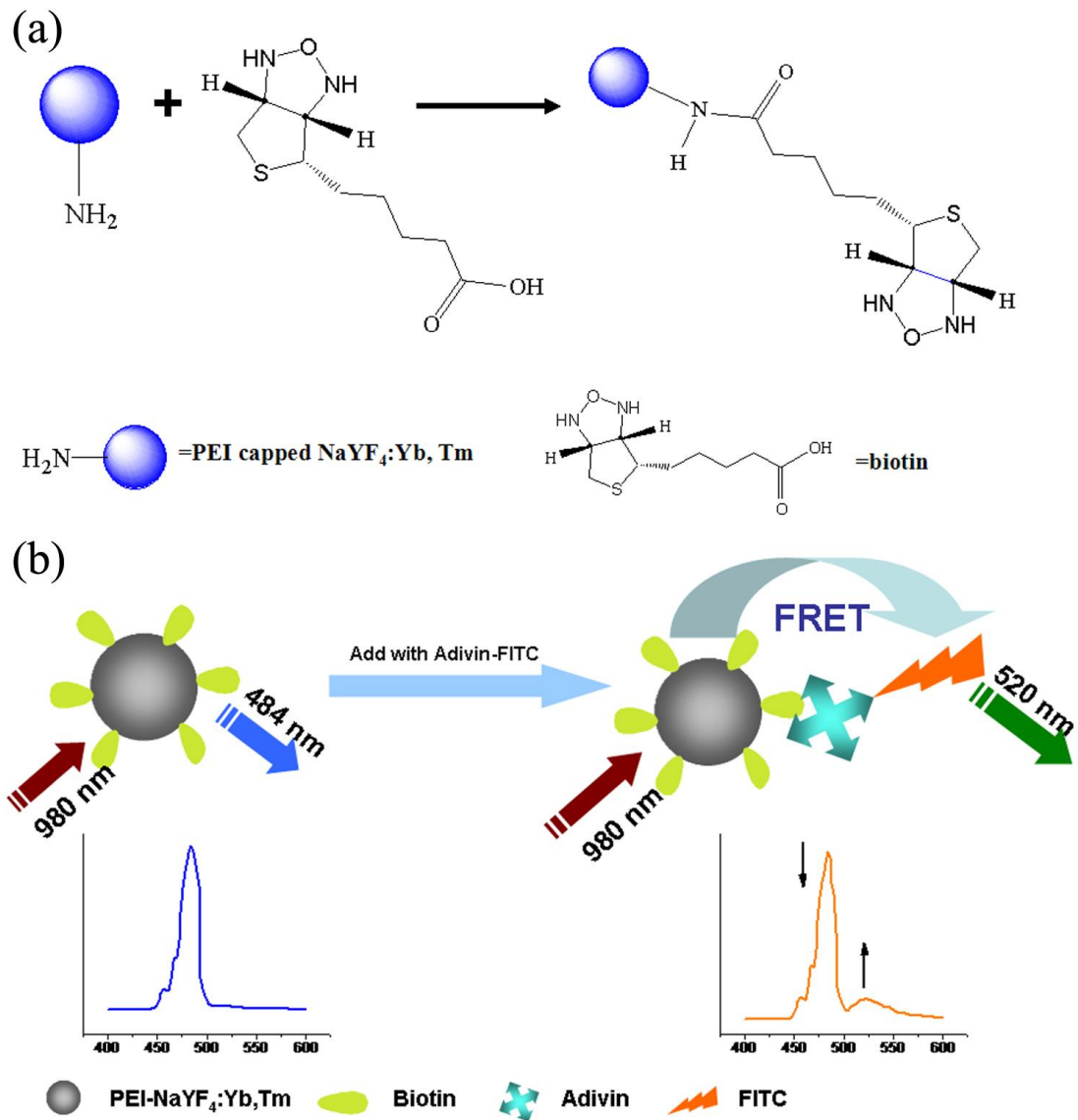
**Figure 11** Photostability of  $\text{NaYF}_4$ : 20% Yb, 0.2% Tm/ $\text{TiO}_2$  UC composite film under continuously illumination by 980 nm laser and  $\text{NaYF}_4$ : 5% Ce, 5% Tb/ $\text{TiO}_2$  DC composite film under continuously illumination by 290 nm lamp for 1h, inset: the emission spectra of the films added with avidin-FITC under excitation of 980 nm laser or 290 nm lamp.

	5 (nm)	7 (nm)	25 (nm)	35 (nm)	50 (nm)
$d_1(\text{NaYF}_4 \text{ film})$	1	1.37	4.24	4.71	4.66
$d_2(\text{Composite})$	1.40	1.84	5.47	5.23	5.31
$d_2/d_1$	1.40	1.34	1.29	1.11	1.14

**Table 1**



Scheme 1



Scheme 2

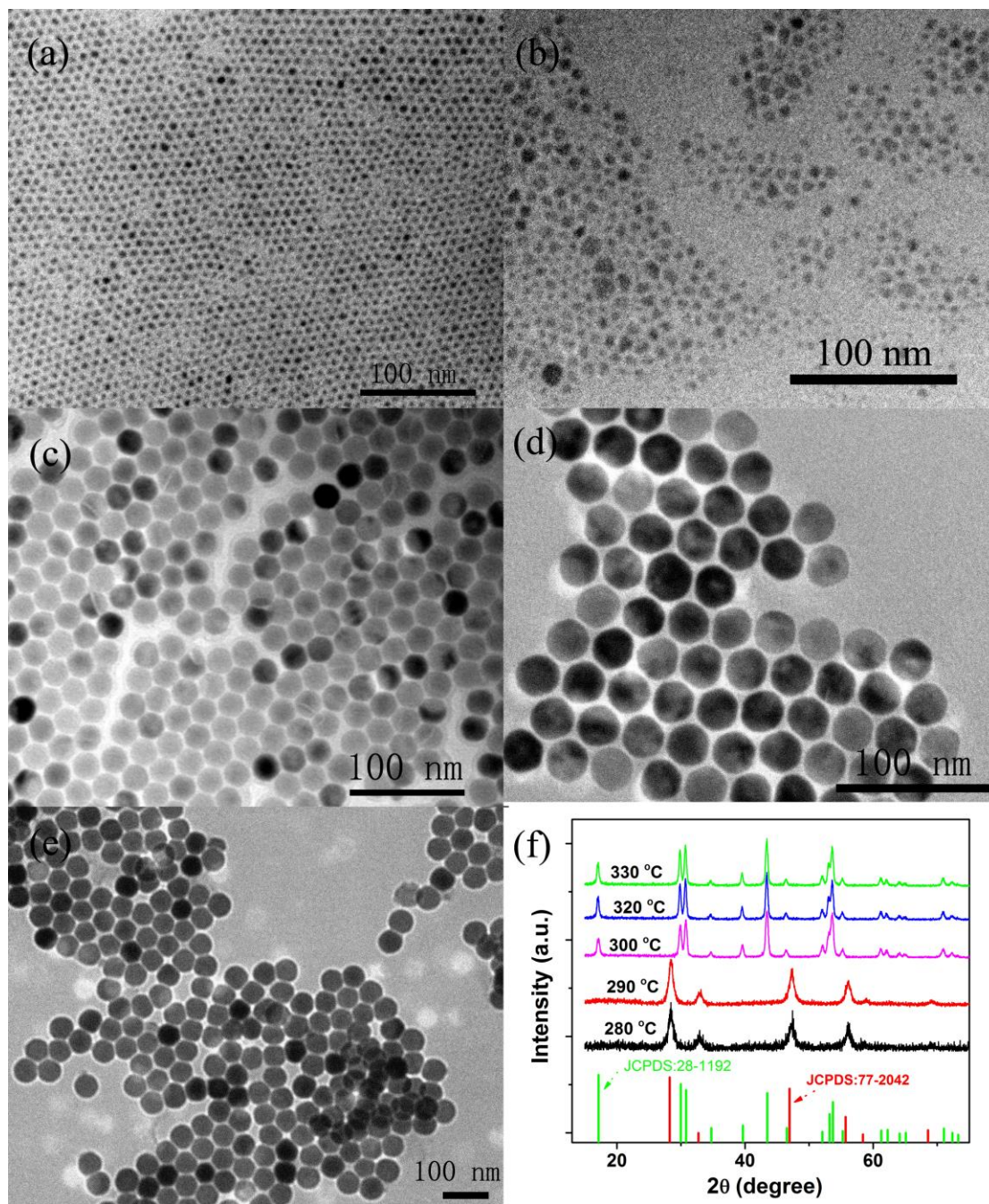


Figure 1

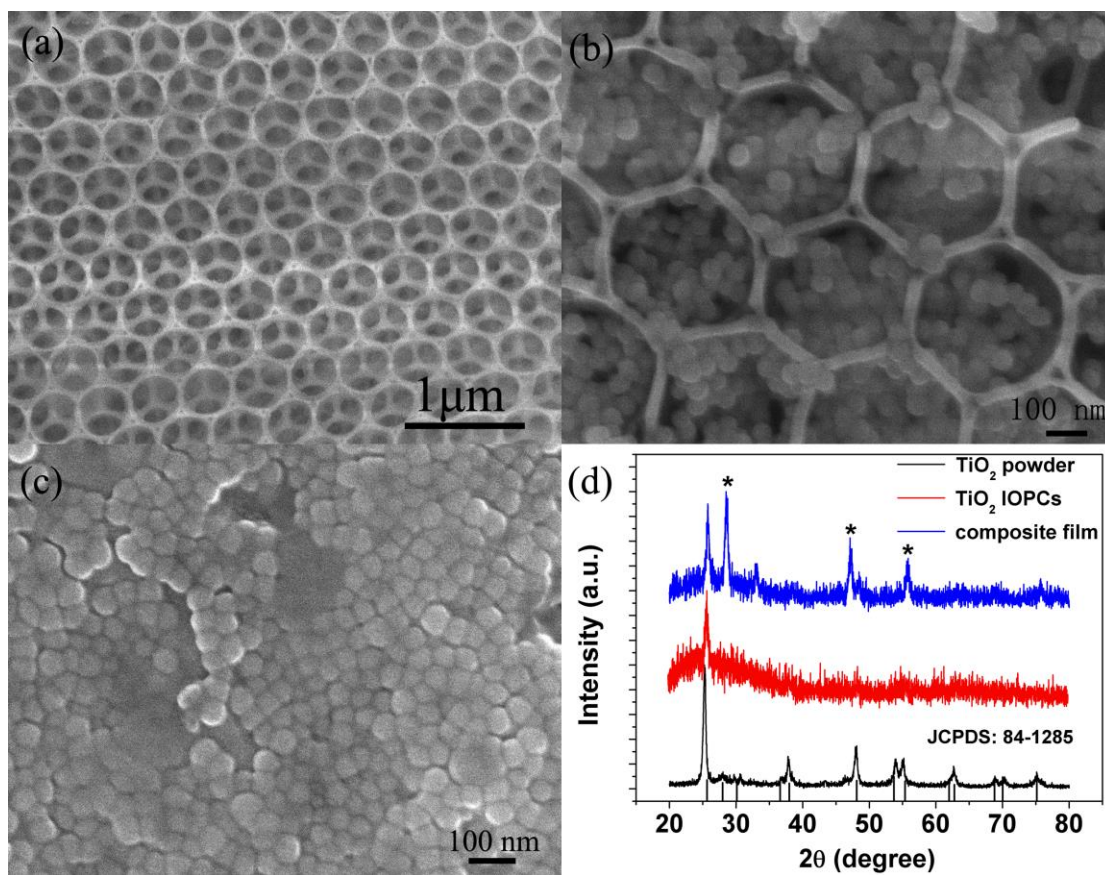


Figure 2

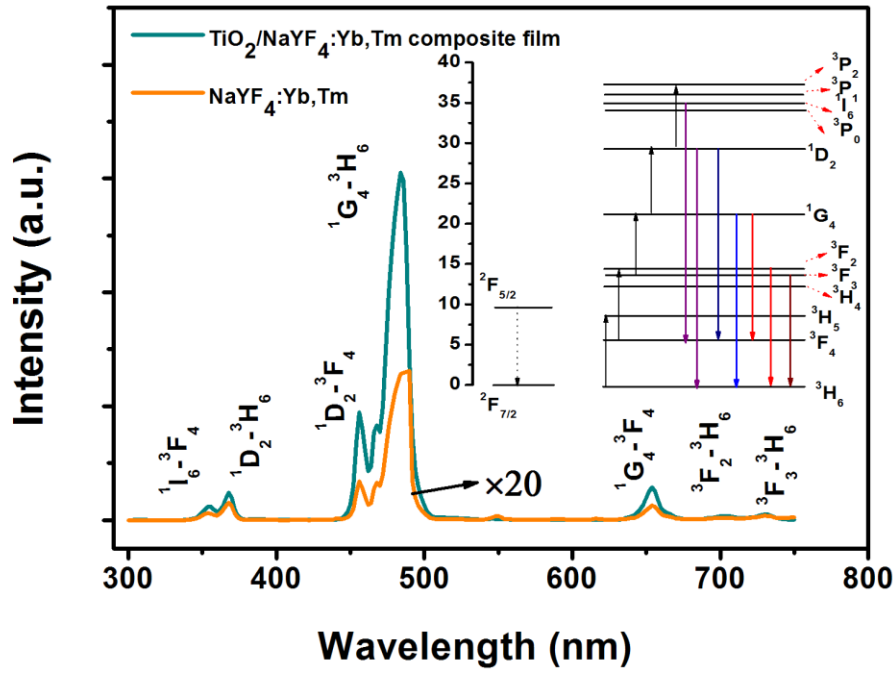


Figure 3

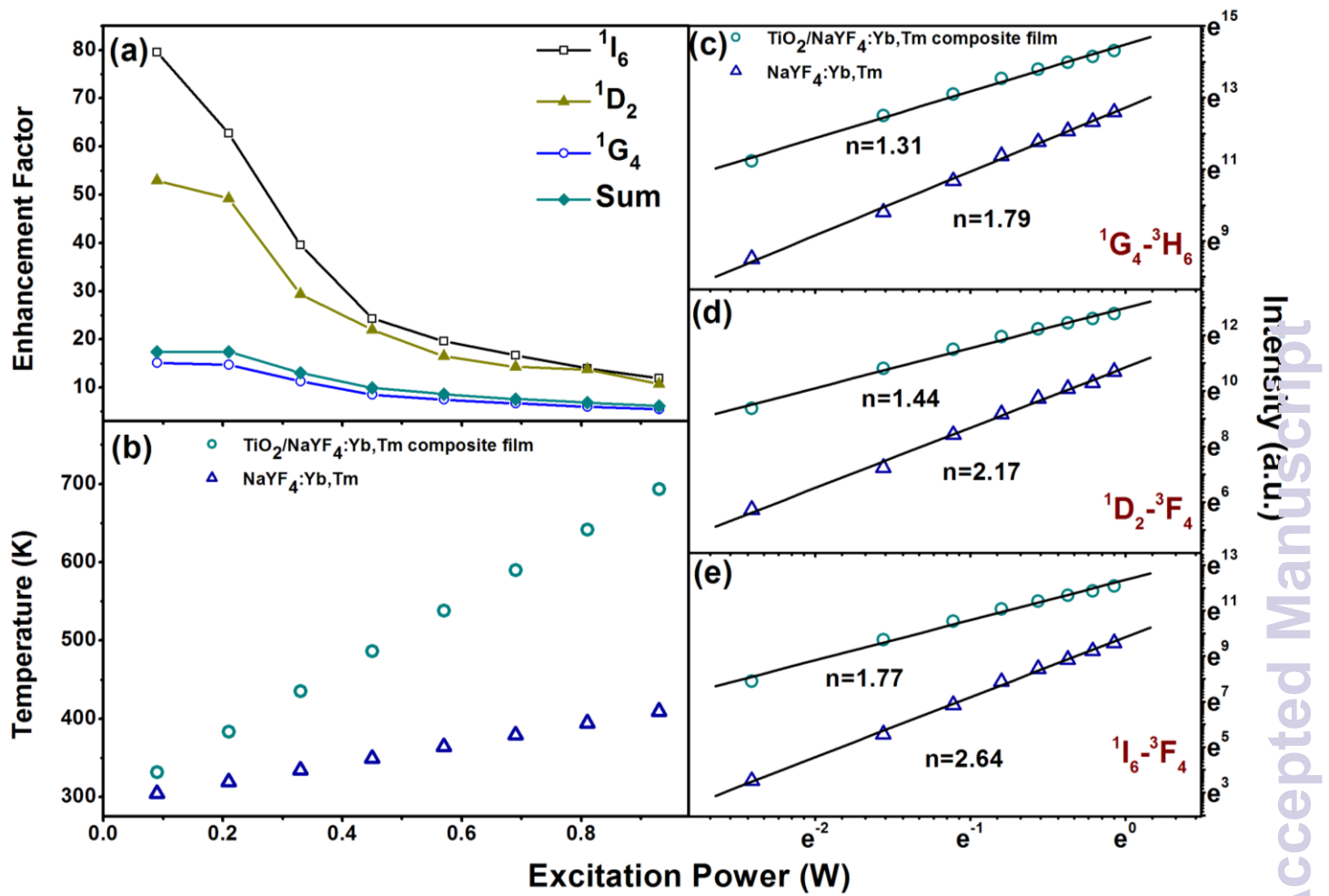


Figure 4

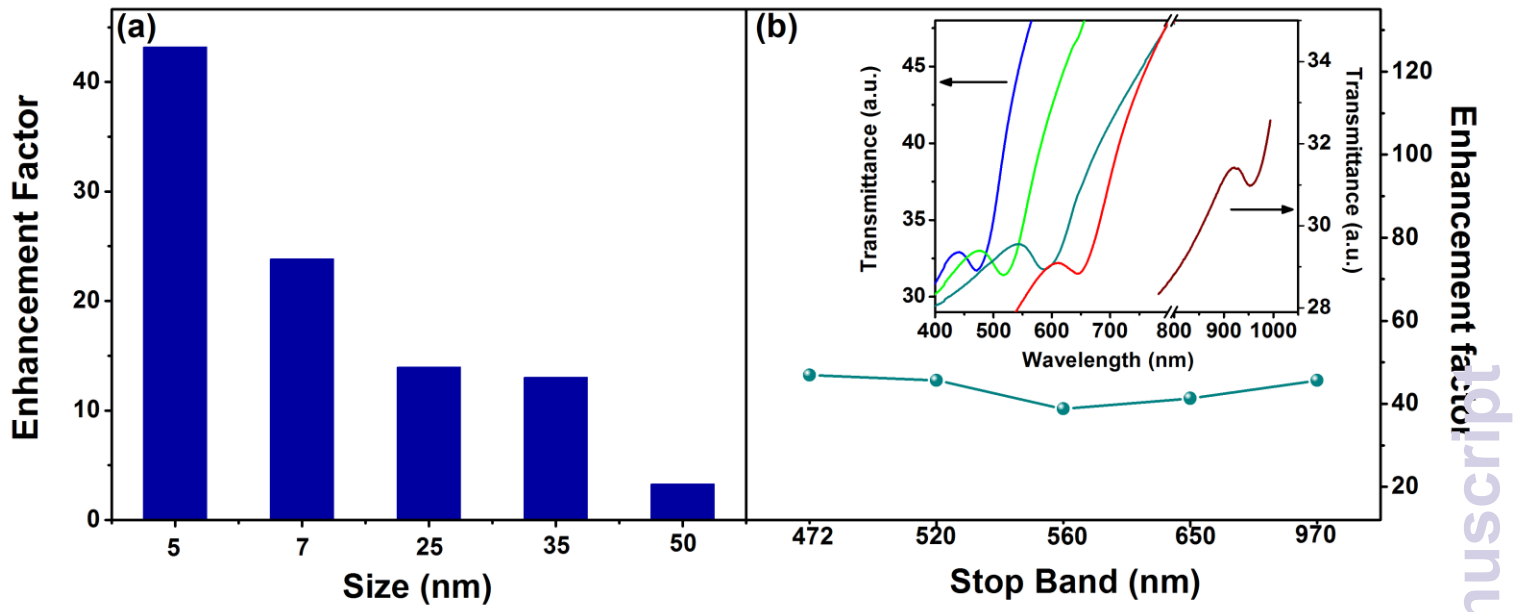


Figure 5

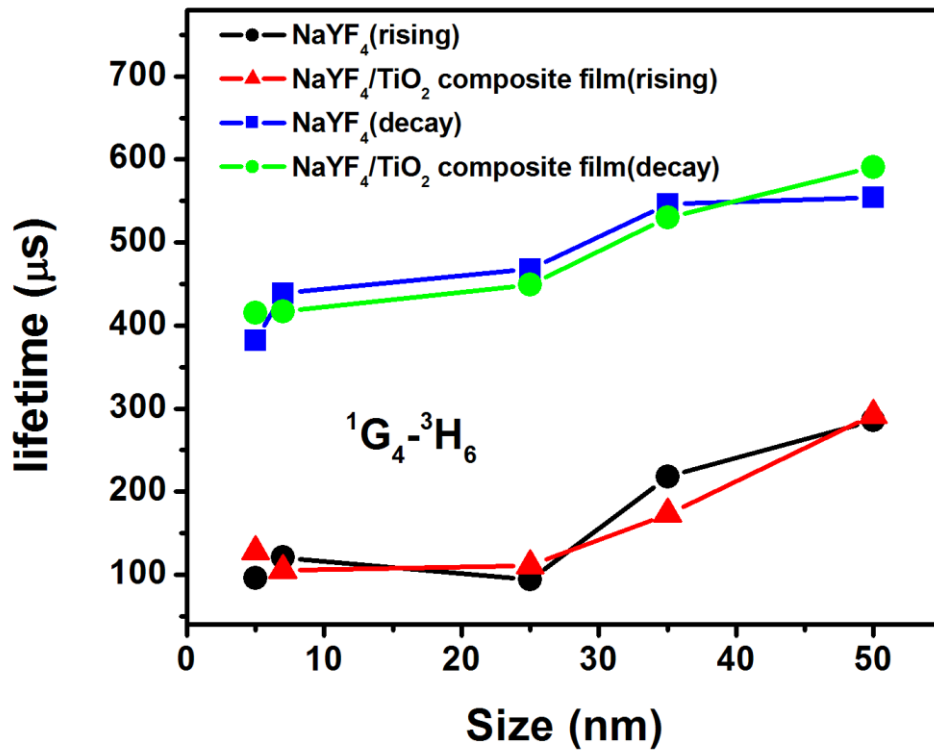


Figure 6

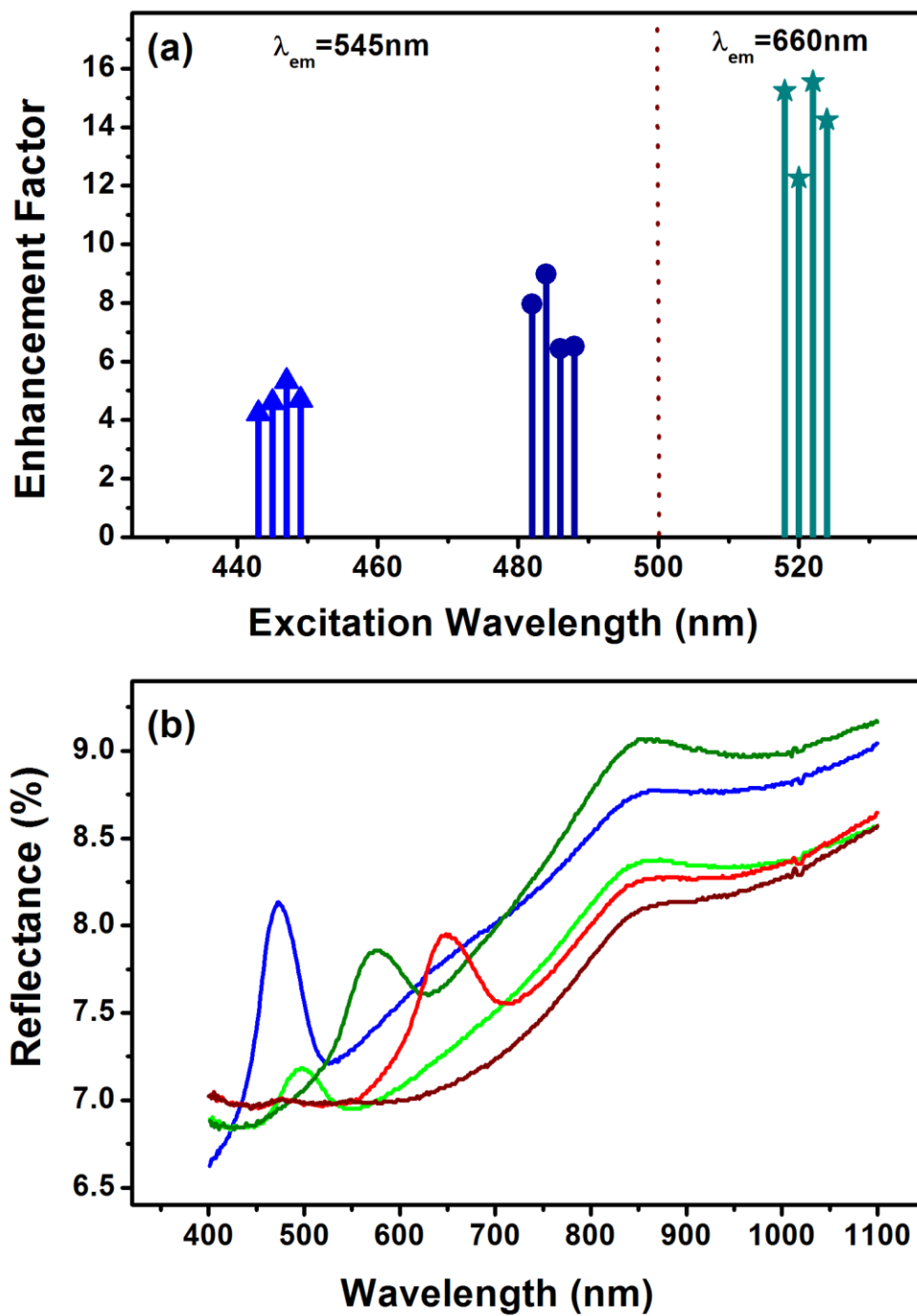


Figure 7

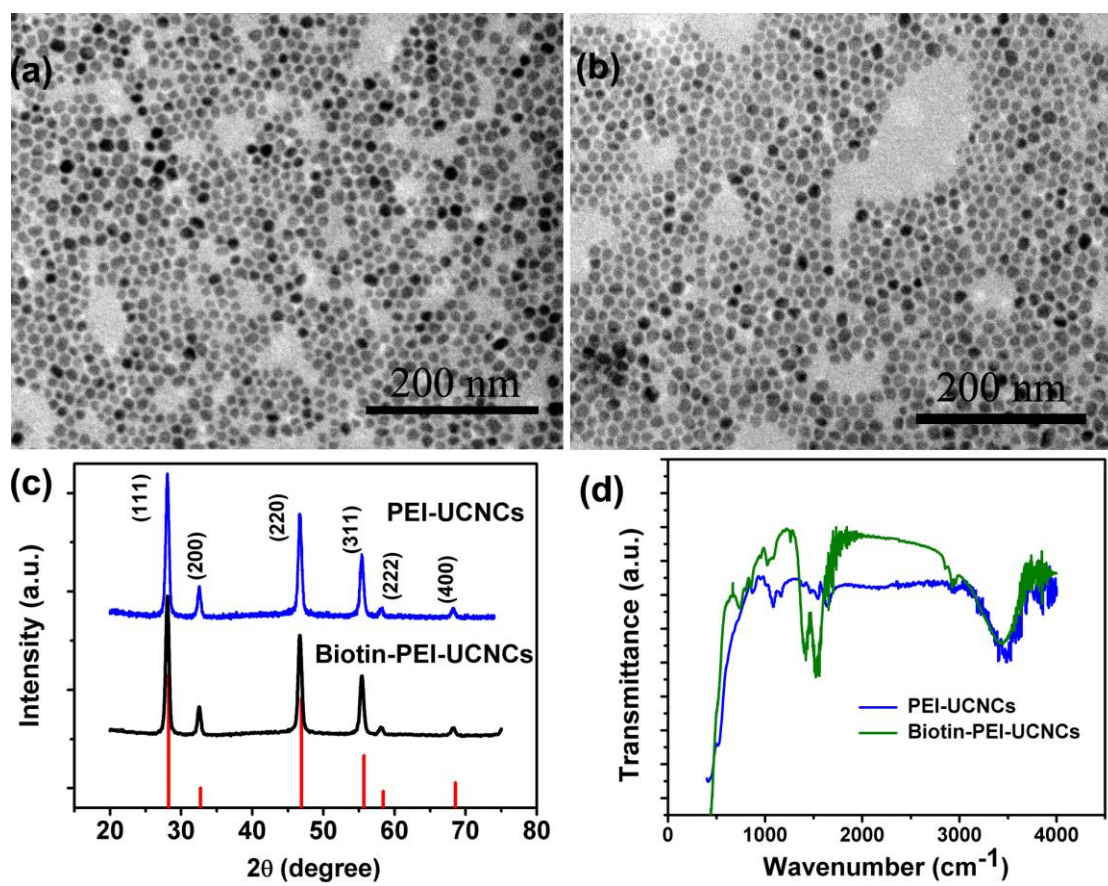


Figure 8

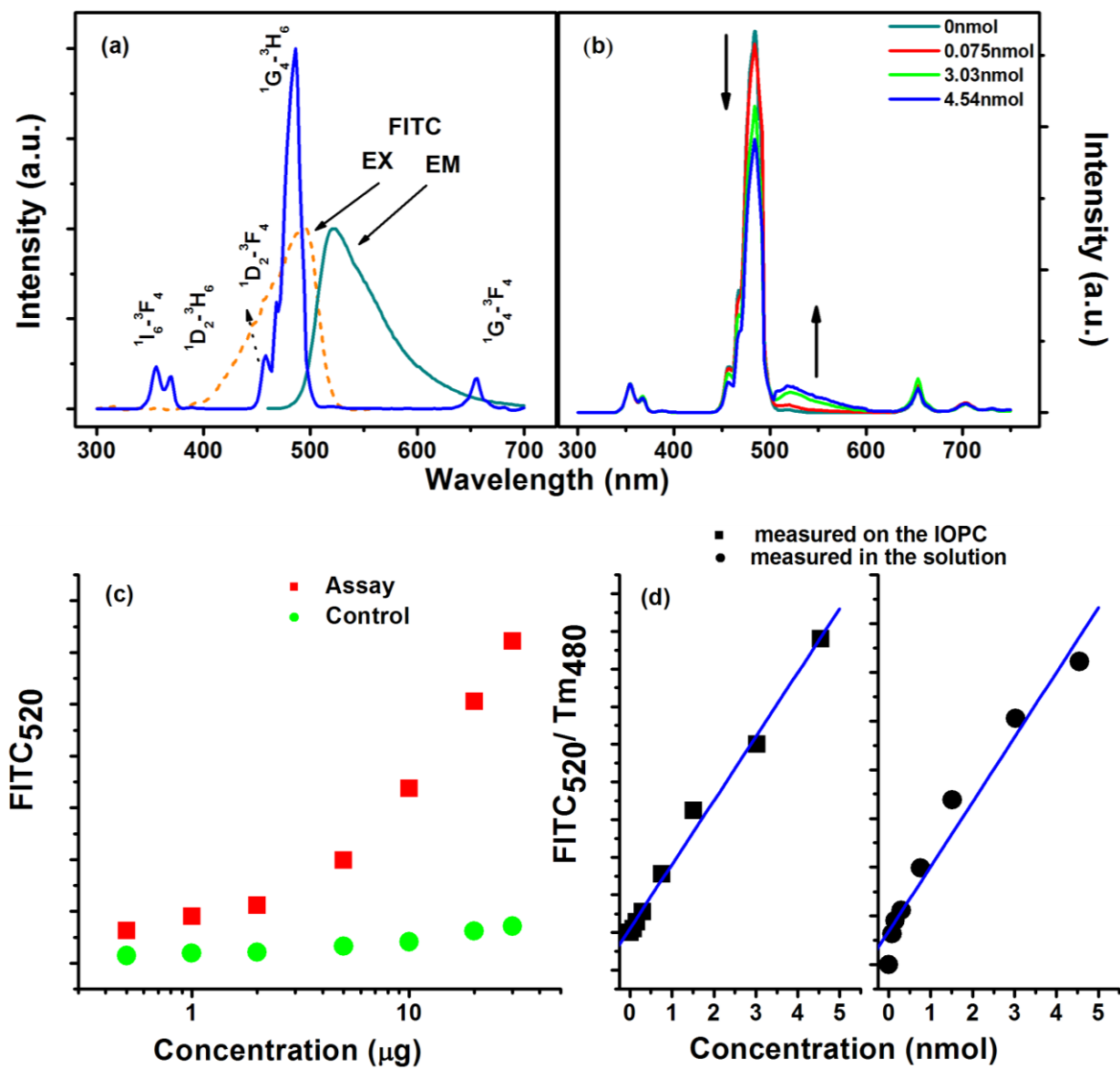


Figure 9

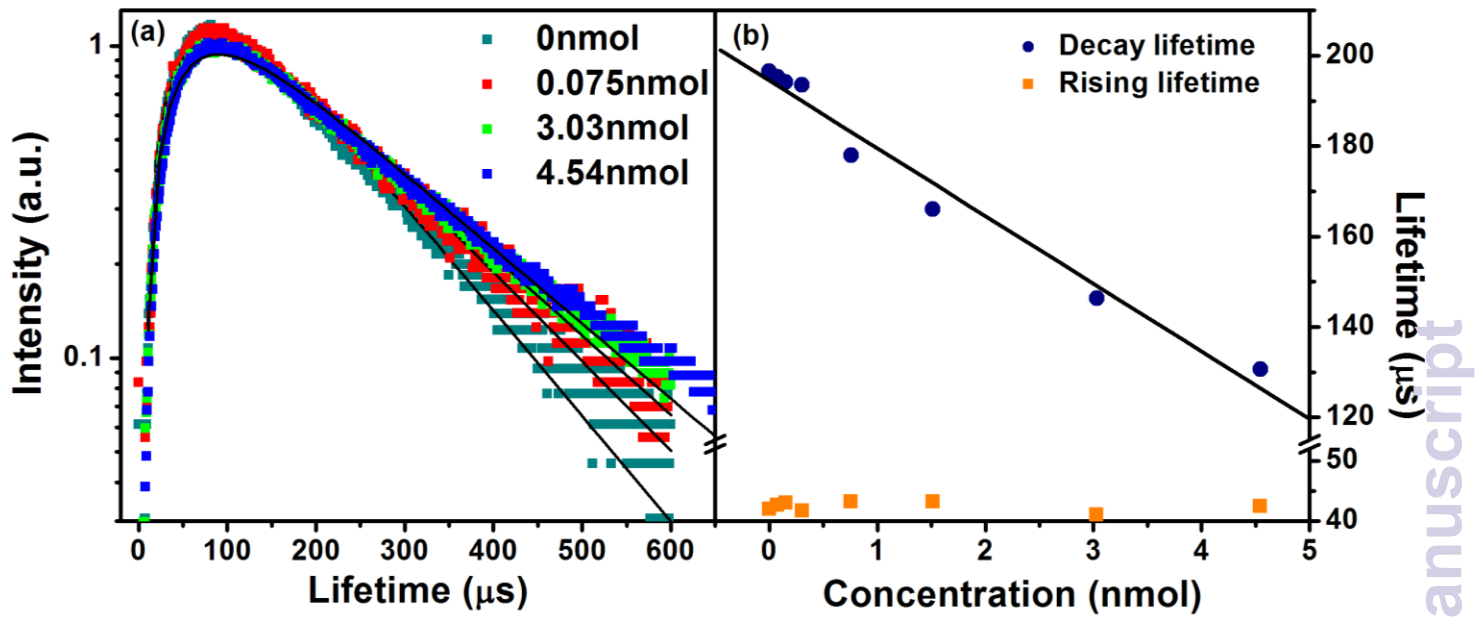


Figure 10

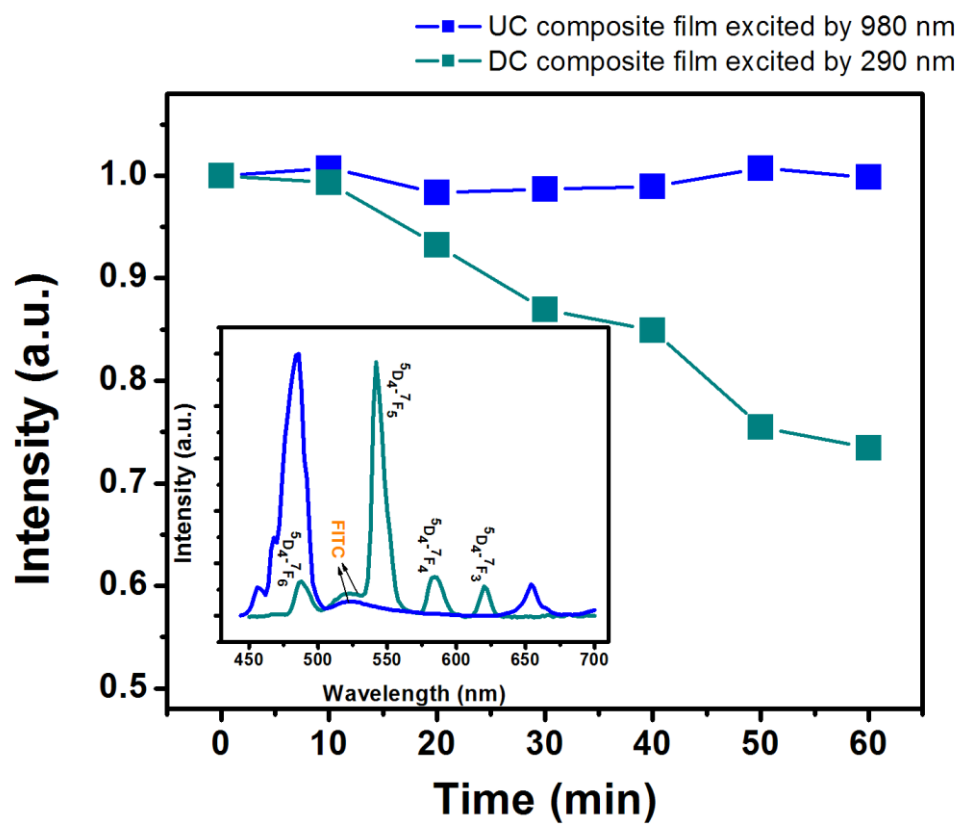


Figure 11